

# Superconductivity and Nematic Fluctuations in a model of FeSe monolayers: A Determinant Quantum Monte Carlo Study

Philipp T. Dumitrescu,<sup>1</sup> Maksym Serbyn,<sup>1</sup> Richard T. Scalettar,<sup>2</sup> Ashvin Vishwanath<sup>1,3</sup>

<sup>1</sup> *Department of Physics, University of California, Berkeley, California 94720, USA*

<sup>2</sup> *Department of Physics, University of California, Davis, CA 95616, USA and*

<sup>3</sup> *Materials Science Division, Lawrence Berkeley National Laboratories, Berkeley, CA 94720, USA*

(Dated: November 28, 2022)

In contrast to bulk FeSe, which exhibits nematic order and low temperature superconductivity, in atomic layers of FeSe the situation is reversed, with high temperature superconductivity appearing along with suppression of nematic order. To investigate this phenomenon, we study a minimal electronic model of FeSe, with interactions that enhance nematic fluctuations. This model is sign problem free, and is simulated using determinant quantum Monte Carlo (DQMC). We developed a DQMC algorithm with parallel tempering, which proves to be an efficient source of global updates and allows us to access the region of strong interactions. Over a wide range of intermediate couplings, we observe superconductivity with an extended s-wave order parameter, along with enhanced, but short ranged,  $q = (0, 0)$  ferro-nematic order. These results are consistent with approximate weak coupling treatments that predict that ferro-nematic fluctuations lead to superconducting pairing. Surprisingly, in the parameter range under study, we do not observe ferro-nematic long range order. Instead, at stronger coupling an unusual insulating phase with  $q = (\pi, \pi)$  *antiferro*-nematic order appears, which are missed by the weak coupling approximations.

PACS numbers: 05.30.Rt, 74.25.Dw, 74.70.Xa, 74.40.Kb

*Introduction.*— A remarkable recent development has been the observation of enhanced superconductivity in single layers of FeSe, grown initially on SrTiO<sub>3</sub> (STO) substrates [1, 2]. In contrast to bulk FeSe which undergoes a superconducting transition at a relatively low temperature of 6 K [3],  $T_c$  in monolayers is at least an order of magnitude larger, in excess of 60 K [4] with even higher transition temperatures reported by an unconventional transport measurement [5]. Initial studies attributed the enhancement of superconductivity to coupling between electrons in the FeSe layer and an STO phonon, which was also implicated in creating shadow electron bands observed in angle resolved photoemission experiments [6, 7]. However, such shadow bands are also observed for electrons on the surface of STO itself, which do not superconduct [8]. Furthermore, recent studies have observed enhancement of  $T_c \sim 40$  K in FeSe in the absence of STO substrate – for example by surface electron doping by depositing potassium [9–12], or in the layered material (Li<sub>0.8</sub>Fe<sub>0.2</sub>)OHFeSe [13, 14]. Since the phonon spectra of these materials are entirely different from STO, an alternate mechanism must be at play, which is intrinsic to the FeSe layers. The common element between these and the original FeSe on STO studies is that heavy electron doping leads to a pair of electron like Fermi surfaces [11, 12, 15–18]. Hence we seek a mechanism for superconductivity that is *intrinsic* to the FeSe layers, that is controlled by electron doping. It has been speculated that the even higher  $T_c$  of FeSe on STO is due to a pairing boost arising from the STO phonon [18, 19], in addition to the intrinsic mechanism.

What is the origin of this intrinsic  $T_c$  enhancement? An attractive possibility is nematic fluctuations for the

following reasons (i) Bulk FeSe undergoes a nematic transition at 100K, and is unique in the family of iron pnictides/chalcogenides in not having a proximate magnetic transition. In fact, no magnetic order is observed down to the lowest temperatures [20, 21] (ii) electron doping has been shown to suppress nematic order [18] in K doped FeSe, following which superconductivity appears. (iii) Theoretically, fluctuations of nematic order in the vicinity of the quantum critical point out of the nematic ordered phase, is expected to lead to superconductivity, and this effect is particularly pronounced in 2D [22–24]. However, existing analytical theories have focused on universal aspects of the physics and are unable to capture non-universal aspects that are relevant to experiments. On the other hand, treatments that incorporate details of FeSe band structure and interactions, are necessarily treated approximately [19, 25–27], and may not correctly capture the true phase structure of the system.

In this paper we investigate the role of nematic fluctuations in enhancing superconductivity, by studying a sign problem free model of the FeSe monolayer, using determinant quantum Monte Carlo (DQMC) calculations. We find that the numerically obtained phase diagram differs substantially from that obtained from a Random Phase Approximation (RPA) approximation [26], particularly in the strong coupling limit. At intermediate couplings though, we find a region with substantially enhanced nematic fluctuations, and superconductivity. Although there is no long range ordered nematic, a notable feature is that the maximum enhancement of uniform nematic fluctuations coincides with peak in a superconducting dome. Moreover, we find that superconductivity responds in an essentially asymmetric way to doping:

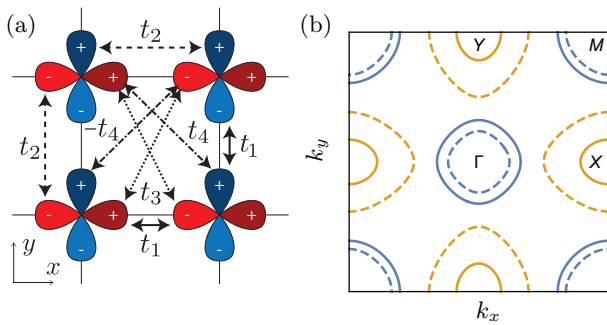


FIG. 1. (a) Definitions of hopping coefficients  $t_{ij}^{ab}$ , where  $d_{xz}$  and  $d_{yz}$  are schematically shown in red/blue color. All hoppings except for  $t_4$  conserve orbital index. (b) Fermi surface for chemical potential  $\mu = 0.6$  (solid lines) and  $\mu = 2$  (dashed lines) at  $g = 0$ , showing two hole pockets at  $\Gamma, M$  and two electron pockets at  $X, Y$ . The hopping values are  $t_1 = -1.0, t_2 = 1.5, t_3 = -1.2, t_4 = -0.95$ . The filling fractions are  $f = 0.43, 0.58$  at  $\mu = 0.6, 2$  respectively.

electron doping enhances superconductivity, while hole doping results in its suppression. All these findings link the emergence of superconductivity to ferro-nematic fluctuations, and are potentially relevant for physics of FeSe films.

Other models recently studied using DQMC have had the order parameter - such as antiferro-magnetism or nematic order, introduced as a separate, dynamic bosonic degree of freedom [28, 29]. While this is appropriate to studying universal aspects of quantum phase transitions, here we will be interested in more microscopic questions. Interestingly, superconductivity was not observed in the effective model considered by [29]. We emphasize that our model defined below includes only electronic degrees of freedom, with properly chosen interactions that are sign problem free. Similar techniques can be used to study many other multi-orbital models, for which the presence of two spin species removes the sign problem at any doping.

*Model.* — We consider a two-band tight binding model, where electrons occupy the  $d_{xz}, d_{yz}$  orbitals of iron atoms on a square lattice. This simplified model captures basic features of the iron pnictide bandstructure [30] and allows for nematic symmetry breaking. We take the Hamiltonian

$$H = - \sum_{ij, ab, \sigma} (t_{ij}^{ab} c_{i a \sigma}^\dagger c_{j b \sigma} + \text{h.c.}) - \mu \sum_{i, a} n_{i, a} - \frac{g}{2} \sum_{\mathbf{i}} (n_{i, xz} - n_{i, yz})^2 \quad (1)$$

where  $a, b = xz, yz$  are orbital indices,  $\sigma = \uparrow, \downarrow$  is the spin index and  $n_{i, a} = \sum_{\sigma} c_{i a \sigma}^\dagger c_{i a \sigma}$  is the occupation of orbital  $a$  on lattice site  $\mathbf{i}$ .

Allowed hopping coefficients  $t_{ij}^{ab}$  are dictated by the

symmetry of the  $d_{xz, yz}$  orbitals and we include hopping between nearest-neighbor ( $t_1, t_2$ ) and next-nearest-neighbor sites ( $t_3, t_4$ ), as shown in Fig. 1(a). The values of  $t_{1, \dots, 4}$  coincide with those used in Ref. [26], and energy will be measured in units of  $t_1$ . The Fermi surface in the non-interacting limit ( $g = 0$ ) with chemical potential  $\mu = 0.6$  consists of two electron pockets at  $X, Y$  and two hole pockets at  $\Gamma, M$  [Fig. 1(b)]. Upon increasing  $\mu$  the hole pocket at  $M$  disappears, while the electron pockets grow.

The attractive interaction term ( $g > 0$ ) in the second line of (1) favors an on-site nematic symmetry by splitting the two orbitals and breaking  $C_4$  rotational symmetry. This is characterized by a non-zero order parameter  $\delta n_{\mathbf{i}} = n_{i, xz} - n_{i, yz}$ . Since the interaction is strictly on-site, the pattern of any nematic ordering is not specified a priori.

The weak coupling Random Phase Approximation (RPA) considers the leading instability of the system from the free fermion susceptibility and predicts a variety of orders for (1), depending on the value of  $\mu$ . In the range  $0.2 < \mu < 2.5$ , including the original parameters considered in Ref. [26], the RPA predicts onset of uniform nematic order for  $g_c \approx 1.7$ . For  $\mu > 2.5$ , the susceptibility peaks at wave-vector  $(0, \pi)$  and  $(\pi, 0)$  predicting stripe order, while for  $\mu < 0.2$  the susceptibility peaks at wave-vector  $(\pi, \pi)$  predicting antiferro-nematic (AFN) [antiferro-quadrupolar (AFQ)] order.

When interactions dominate  $g \gg t, \mu$ , we can get intuition from a strong coupling expansion in  $t/g$ . At zeroth order, the ground state is doubly degenerate – either orbital  $xz$  or  $yz$  are fully occupied on each site. This degeneracy is split by second order processes, leading to nearest- and next-nearest-neighbor Ising-type interactions of order  $\sim t^2/g$ . For our hopping parameters, the ground state of resulting Ising model is a checkerboard pattern [31] – this corresponds to AFN order at half-filling ( $f = 0.5$  electrons per site per orbital per spin). On the other hand, intuition from anti-ferromagnetic order in the half-filled Hubbard model [32] suggests that doping will quickly destroy this checkerboard order.

The sensitivity of the weak coupling instability to  $\mu$ , along with the instability of AFN order with respect to doping away from half filling suggest a number of competing orders and we proceed to study the phase diagram of (1) numerically.

*Sign-problem-free DQMC.* — We simulate the model in an unbiased fashion using Determinant Quantum Monte Carlo (DQMC) with discretized time-steps as described in [33–35]. In order to sample the full imaginary time partition function  $Z = \text{Tr} e^{-\beta H}$ , we decouple the interactions in the nematic channel using a continuous auxiliary Hubbard-Stratonovich field  $\varphi$ . Integrating out the fermions analytically, the partition function becomes a path integral of the auxiliary field,  $Z = \int D\varphi e^{-S_b(\varphi)} \text{Det} G^{-1}(\varphi)$ , and can be sampled using the

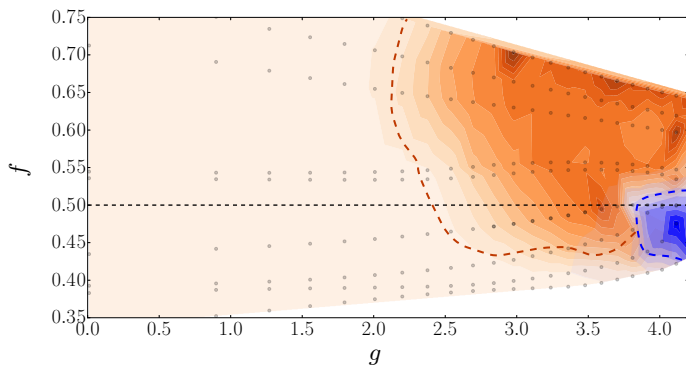


FIG. 2. Phase diagram of the model (1) as a function of interaction  $g$  and filling fraction  $f$  at inverse temperature  $\beta = 8$ . The red dashed line indicates the boundary of the region where the superconducting order parameter extrapolates to a finite value in the thermodynamic limit. The blue dashed line marks the boundary of phase with antiferro-nematic order. The red / blue coloring is the interpolated equal time correlation function of the s-wave superconductivity / antiferro-nematic order on a  $10 \times 10$  lattice; white space is outside of range sampled. Dots indicate simulated points along 10 values of the chemical potentials  $\mu = -1, \dots, 4$ . The black dashed line marks half filling.

Metropolis Monte Carlo algorithm. The fermion determinant  $\text{Det } G^{-1}(\varphi)$  decouples into spin sectors since the kinetic energy does not mix spins and  $\varphi_i$  couples equally to  $\uparrow, \downarrow$  through  $\delta n_i$ . The spin sectors are equal by time reversal for any field configuration  $\varphi$ ,  $\text{Det } G^{-1}(\varphi) = \text{Det } G_{\uparrow}^{-1}(\varphi) \text{Det } G_{\downarrow}^{-1}(\varphi) = |\text{Det } G_{\uparrow}^{-1}(\varphi)|^2 > 0$ , which guarantees that the partition function can be sampled in a sign-problem-free manner at any filling.

We perform sweeps through the space-time lattice and update the Hubbard-Stratonovich field  $\varphi$  on each site. As  $\varphi$  couples different orbitals, we perform rank-two Woodbury updates [36] when calculating  $G_{\uparrow}$  on a given time-slice. We use the one-sided Jacobi Singular-Value Decomposition algorithm [37] for numerical stabilization [38] on every second time-slice. In order to reduce ergodicity problems at strong interactions, we run the DQMC simulation in parallel for various interactions and use a parallel-tempering algorithm [39], which proposes to exchange  $\varphi$  configurations between simulations at different interaction strength  $g$  after each sweep [40]. For the data presented here, we have simulated systems with periodic boundary conditions up to  $L^2 = 10 \times 10$  in spatial size (200 orbitals) with an inverse temperature of up to  $\beta = 8$  ( $\beta E_F \sim 40$ ); the imaginary time step is  $\Delta\tau = 1/16$ .

*Phase diagram.*— We mapped the phase diagram of model (1) as a function of interaction strength  $g$  and filling fraction  $f$  (Fig. 2), showing regions of superconducting and antiferro-nematic order. We are considering a finite temperature system in two spatial dimensions, so only quasi-long-range order exists. Since our simulations are on lattice sizes smaller than the scale of these fluctu-

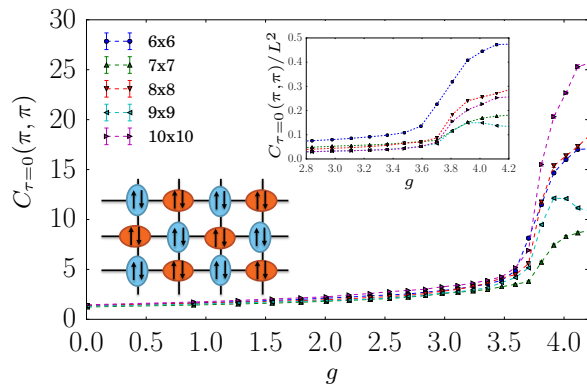


FIG. 3. Equal time nematic correlation function averaged around  $q = (\pi, \pi)$  rises rapidly, signaling onset of the long-range order. The left inset shows a cartoon of the antiferro-nematic ordering pattern. The second inset indicates the convergence of the correlation function, when normalized by  $L^2$ , as expected from long-range order. Note the even-odd effect due to periodic boundary conditions.

ations, our finite size extrapolations indicate long range order of the  $T = 0$  ground state.

We first discuss the phase diagram in vicinity of half-filling  $f = 0.5$ , which corresponds to two electrons per site. In the limit of strong coupling  $g \geq 3.75$  we see development of long-range antiferro-nematic order. This is fully consistent with the intuition from the strong coupling expansion of a fully polarized state in the orbital basis with a checkerboard ordering pattern (Fig. 3 inset). The onset of order is confirmed by considering the growth of the equal time nematic correlation function

$$C_{\tau=0}(\mathbf{q}) = \frac{1}{L^2} \sum_{\mathbf{i}, \mathbf{j}} e^{i\mathbf{q} \cdot (\mathbf{i} - \mathbf{j})} \langle \delta n_{\mathbf{i}} \delta n_{\mathbf{j}} \rangle. \quad (2)$$

The behavior of  $C_{\tau=0}(\mathbf{q})$  at  $q = (\pi, \pi)$  is shown in Fig. 3. To reduce finite size effects, we show  $C_{\tau=0}(\mathbf{q})$  averaged over three neighboring points  $\mathbf{q}, \mathbf{q} + 2\pi/L\mathbf{e}_x, \mathbf{q} + 2\pi/L\mathbf{e}_y$  which coincide in the thermodynamic limit. We also confirmed the onset of order via the Binder ratio [41] for the boson field conjugate to  $\delta n$  at zero frequency (not shown).

The AFN order rapidly disappears when the system is doped away from half-filling, or the interaction strength is decreased. In contrast to the expectations from weak coupling RPA, we do not observe any nematic ordering at other wave-vectors. Instead, when the long range AFN disappears, we observe a large region with non-zero superconducting order. In order to probe the superconducting order, we study the equal-time pair correlation function  $\sim \langle \Delta_{ab}(i) \Delta_{cd}^\dagger(j) \rangle$ , where the specific form of the  $\Delta_{ab}(i)$  depends on the symmetry of pairing. We consider all possible irreducible representations of lattice point group  $D_4$  involving on-site, nearest neighbor and

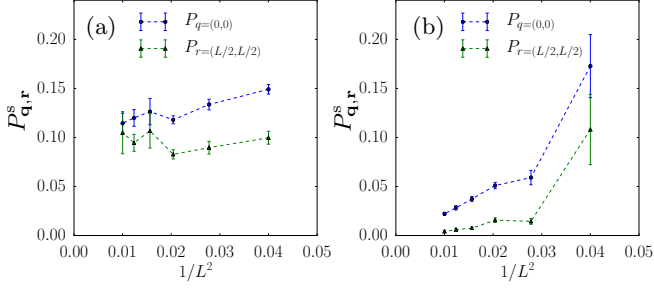


FIG. 4. Finite size scaling of the on-site s-wave equal time pair correlation at maximal-distance  $P_{\mathbf{r}=(L/2,L/2)}^s$  and zero-momentum  $P_{\mathbf{q}=0}^s$ . (a) In the region which we identify as a superconductor ( $\mu = 0.6$ ,  $g = 3.59$ )  $P_{\mathbf{r}}, P_{\mathbf{q}}$  extrapolate to a finite value in the thermodynamic limit. (b) In the region of the AFN phase ( $\mu = 0.6$ ,  $g = 3.91$ ), the pair correlation functions scale to zero in the thermodynamic limit.

next nearest neighbor sites and found non-vanishing pair correlation function for the order parameter with s-wave ( $A_1$ ) symmetry. The dominant response is the on-site pairing, where the only non-vanishing pairing is within the same orbitals with equal sign ( $A_1 \times A_1$  irreducible representation),

$$\Delta^s(\mathbf{i}) = \frac{1}{2} c_{i\alpha\alpha} (i\sigma_{\alpha\beta}^y) (\tau_{ab}^0) c_{ib\beta}. \quad (3)$$

Here  $\sigma$  and  $\tau$  are the Pauli matrices acting in the spin and orbital basis, and  $\tau^0$  is an identity matrix. The order parameter  $\Delta^s(\mathbf{i})$  coexists with the extended s-wave pairing between nearest neighbors,  $\Delta^{s\text{-ex}}(\mathbf{i})$ , where the gap changes sign between orbitals ( $B_1 \times B_1$  representation),

$$\Delta^{s\text{-ex}}(\mathbf{i}) = \frac{1}{2} \sum_{\hat{e}} d(\hat{e}) c_{i+\hat{e},\alpha\alpha} (\sigma_{\alpha\beta}^y) (\tau_{ab}^z) c_{ib\beta}, \quad (4)$$

as is reflected by  $\tau^z$  matrix. In these notations vector  $\hat{e}$  runs over nearest neighbors and  $d(\hat{e})$  denotes the  $d_{x^2-y^2}$ -wave symmetry form-factor,  $d(\pm\hat{x}) = 1$ , and  $d(\pm\hat{y}) = -1$ . For  $\mu \geq 2$ , the extended s-wave pairing also extends to the next nearest neighbor sites (along diagonals) for and has a  $d_{xy}$ -wave form factor along with the  $\tau^x$  pairing in the orbital basis ( $B_2 \times B_2$  representation).

The equal time ( $\tau = 0$ ) pair correlation function for the on-site s-wave is defined as

$$P_{\mathbf{r}}^s = \frac{1}{L^2} \sum_{\mathbf{i}} \langle \Delta^s(\mathbf{i} + \mathbf{r}) \Delta^s(\mathbf{i}) \rangle, \quad P_{\mathbf{q}}^s = \frac{1}{L^2} \sum_{\mathbf{r}} e^{i\mathbf{q}\cdot\mathbf{r}} P_{\mathbf{r}}^s \quad (5)$$

in the coordinate and Fourier space respectively, where both sums are performed over all lattice points. In the thermodynamic limit the value  $P_{\mathbf{q}}^s$  at  $\mathbf{q} = 0$  must converge to the pair correlation function at the maximum

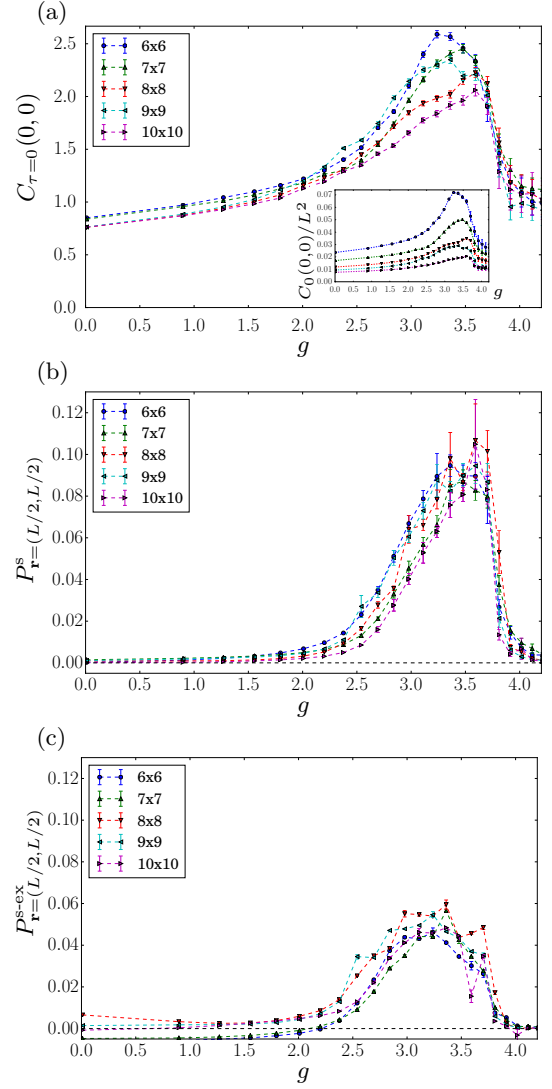


FIG. 5. The (a) uniform nematic correlation function, (b) on-site s-wave pair correlation function, and (c) nearest neighbor extended s-wave have very similar dependence on the interaction strength for fixed value of  $\mu = 0.6$ . The onset and termination of on-site superconducting order coincides with the similar trends in nematic susceptibility. In (a), the insert shows the correlation function normalized by  $1/L^2$  showing the decrease with system size and lack of long-range order.

separation  $P_{\mathbf{r}, \mathbf{r}=(L/2,L/2)}^s$ , provided there is long-range superconducting order. At small  $L$ ,  $P_{\mathbf{q}=0}^s$  includes mostly short range contributions and overestimates the order parameter. Figure 4(a) demonstrates a case where both quantities extrapolate to finite value as  $1/L \rightarrow 0$ , moreover these quantities become closer to each other for larger system sizes as expected. In contrast, in the AFN phase, the pair correlation function is non-zero only due to finite size effects and extrapolate to zero in the thermodynamic limit, see Fig. 4(b).

*Origin of superconductivity.*— We observed an ex-

tended s-wave superconducting order in a large portion of the phase diagram. One may worry that this superconducting order arises only from the attractive parts of the interaction in the model defined by (1). However, decoupling the interaction in the pairing channel within a mean field calculation only leads to significant superconducting pairing for much stronger interactions,  $g \geq 6$  at  $\beta = 8$ . Since the mean field approximation tends to overestimate the ordering tendency, this suggests that this scenario is improbable.

A number of recent works [22, 24] addressed enhancement of superconductivity in a vicinity of a uniform nematic transition by nematic fluctuations. While we do not find long-range uniform nematic order in the considered range of dopings/interactions, the intuition from weak-coupling RPA suggests possible competition between various ordering tendencies for this model. Then, upon approaching the AFN transition, we expect to have enhancement of fluctuations in various channels, including uniform nematic fluctuations.

To check if the uniform nematic fluctuations play a role in the superconducting phase, we compare the evolution of equal time nematic and pair correlation functions with interactions, Fig. 5(a)-(c). The uniform nematic correlation function has a maximum around  $g \approx 3.5$ , exactly where  $P_{\mathbf{r}}^s$  peaks. For larger interaction, the onset of the AFN phase signaled by a rapid increase in AFN correlations for  $g \geq 3.7$  (see Fig. 3) coincides with the destruction of superconductivity and suppression of uniform nematic correlations.

*Discussion and implications for FeSe.*—Our studies of the purely electronic model with interactions in nematic channel revealed a phase diagram with large superconducting region. While our two-band model is oversimplified, it roughly captures the behavior of FeSe Fermi surface with doping: electron pockets increase in size upon doping, while hole pockets shrink. Moreover, we use a local on-site interaction that favors imbalance in orbital occupancy. Similar interaction terms were shown to arise from the Fe-ion oscillations [42], so we consider our interaction term as an approximation after one integrates out high energy bosonic mode. The on site Coulomb repulsion, which is absent in our model, will presumably suppress on site pairing, but the extended parts of the superconducting pairing, which we find share the same trends as the onsite pairing, will presumably be less affected, and may be directly relevant for the observed superconductivity in FeSe films.

Our model in Eq. (1) was found to have a long-range antiferro-nematic order at strong coupling, whereas the bulk FeSe is believed to have a uniform nematic order. Nevertheless, the model considered here has enhanced uniform nematic fluctuations as a precursor to the onset of uniform order. We found that these nematic fluctuations are correlated with enhancement of superconductivity. Moreover, we observed an essential asymmetry

of the superconducting phase, doping with electrons enhances superconducting order, while hole doping destroys it. This is consistent with the phenomenology of FeSe, where SC emerges upon strong electron doping. One can potentially try to connect the nematic fluctuation mechanism more closely with the observed superconductivity by looking for anisotropy of the gaps in momentum space [24], which is left for future work on larger system sizes.

We found an extended s-wave superconducting order, where the leading contribution is an on-site pairing diagonal in the orbital basis. The next contributions have a d-wave pattern in a real space and have non-trivial character in the orbital basis.

To conclude, we proposed a two band model with interactions which enhance nematic fluctuations and studied this model using DQMC. We find that robust high temperature superconductivity appears that is accompanied by ferro-nematic fluctuations, although the ferro-nematic ordered phase itself does not appear in the range that was studied. Our findings can be relevant to enhanced superconductivity in FeSe films, as well as other situations where a fluctuating order may be responsible for superconductivity. Our methods are readily extendible to a wide class of multi-orbital models.

*Acknowledgments.*— We thank S. Gazit for numerous discussions. This research was supported by the Gordon and Betty Moore Foundation EPiQS Initiative through Grant GBMF4307 (M.S.), the U.S. Department of Energy, Office of Science, Office of Basic Energy Sciences under DE-SC0014671 (R.T.S.) and a Simons Investigator grant (A.V.).

*Note added.*— During completion of this work, references [43–45] appeared, which find superconductivity on applying DQMC to different models. In contrast to those works which couple electrons to bosonic (typically spin density waves) modes with intrinsically defined dynamics, here we are concerned with a purely electronic model and focus on nematic fluctuations.

- 
- [1] W. Qing-Yan, L. Zhi, Z. Wen-Hao, Z. Zuo-Cheng, Z. Jin-Song, L. Wei, D. Hao, O. Yun-Bo, D. Peng, C. Kai, W. Jing, S. Can-Li, H. Ke, J. Jin-Feng, J. Shuai-Hua, W. Ya-Yu, W. Li-Li, C. Xi, M. Xu-Cun, and X. Qi-Kun, *Chinese Physics Letters* **29**, 037402 (2012).
  - [2] D. Liu, W. Zhang, D. Mou, J. He, Y.-B. Ou, Q.-Y. Wang, Z. Li, L. Wang, L. Zhao, S. He, Y. Peng, X. Liu, C. Chen, L. Yu, G. Liu, X. Dong, J. Zhang, C. Chen, Z. Xu, J. Hu, X. Chen, X. Ma, Q. Xue, and X. J. Zhou, *Nat Commun* **3**, 931 (2012).
  - [3] F.-C. Hsu, J.-Y. Luo, K.-W. Yeh, T.-K. Chen, T.-W. Huang, P. M. Wu, Y.-C. Lee, Y.-L. Huang, Y.-Y. Chu, D.-C. Yan, and M.-K. Wu, *Proceedings of the National Academy of Sciences* **105**, 14262 (2008).
  - [4] Z. Zhang, Y.-H. Wang, Q. Song, C. Liu, R. Peng,

- K. Moler, D. Feng, and Y. Wang, *Science Bulletin* **60**, 1301 (2015).
- [5] J.-F. Ge, Z.-L. Liu, C. Liu, C.-L. Gao, D. Qian, Q.-K. Xue, Y. Liu, and J.-F. Jia, *Nat Mater* **14**, 285 (2015).
- [6] J. J. Lee, F. T. Schmitt, R. G. Moore, S. Johnston, Y. T. Cui, W. Li, M. Yi, Z. K. Liu, M. Hashimoto, Y. Zhang, D. H. Lu, T. P. Devereaux, D. H. Lee, and Z. X. Shen, *Nature* **515**, 245 (2014).
- [7] R. Peng, H. C. Xu, S. Y. Tan, H. Y. Cao, M. Xia, X. P. Shen, Z. C. Huang, C. H. P. Wen, Q. Song, T. Zhang, B. P. Xie, X. G. Gong, and D. L. Feng, *Nat Commun* **5** (2014).
- [8] C. Chen, J. Avila, E. Frantzeskakis, A. Levy, and M. C. Asensio, *Nat Commun* **6** (2015).
- [9] C. H. P. Wen, H. C. Xu, C. Chen, Z. C. Huang, Y. J. Pu, Q. Song, B. P. Xie, M. Abdel-Hafeez, D. A. Chareev, A. N. Vasiliev, R. Peng, and D. L. Feng, ArXiv e-prints (2015), [arXiv:1508.05848 \[cond-mat.supr-con\]](#).
- [10] C. H. P. Wen, H. C. Xu, C. Chen, Z. C. Huang, Y. J. Pu, Q. Song, B. P. Xie, M. Abdel-Hafeez, D. A. Chareev, A. N. Vasiliev, R. Peng, and D. L. Feng, ArXiv e-prints (2015), [arXiv:1508.05848 \[cond-mat.supr-con\]](#).
- [11] Y. Miyata, K. Nakayama, K. Sugawara, T. Sato, and T. Takahashi, *Nat Mater* **14**, 775 (2015).
- [12] C. Tang, C. Liu, G. Zhou, F. Li, D. Zhang, Z. Li, C. Song, S. Ji, K. He, X. Chen, L. Wang, X. Ma, and Q.-K. Xue, ArXiv e-prints (2015), [arXiv:1508.06368 \[cond-mat.supr-con\]](#).
- [13] X. F. Lu, N. Z. Wang, H. Wu, Y. P. Wu, D. Zhao, X. Z. Zeng, X. G. Luo, T. Wu, W. Bao, G. H. Zhang, F. Q. Huang, Q. Z. Huang, and X. H. Chen, *Nat Mater* **14**, 325 (2015).
- [14] H. Sun, D. N. Woodruff, S. J. Cassidy, G. M. Allcroft, S. J. Sedlmaier, A. L. Thompson, P. A. Bingham, S. D. Forder, S. Cartenet, N. Mary, S. Ramos, F. R. Foronda, B. H. Williams, X. Li, S. J. Blundell, and S. J. Clarke, *Inorganic Chemistry* **54**, 1958 (2015).
- [15] S. He, J. He, W. Zhang, L. Zhao, D. Liu, X. Liu, D. Mou, Y.-B. Ou, Q.-Y. Wang, Z. Li, L. Wang, Y. Peng, Y. Liu, C. Chen, L. Yu, G. Liu, X. Dong, J. Zhang, C. Chen, Z. Xu, X. Chen, X. Ma, Q. Xue, and X. J. Zhou, *Nat Mater* **12**, 605 (2013).
- [16] S. Tan, Y. Zhang, M. Xia, Z. Ye, F. Chen, X. Xie, R. Peng, D. Xu, Q. Fan, H. Xu, J. Jiang, T. Zhang, X. Lai, T. Xiang, J. Hu, B. Xie, and D. Feng, *Nat Mater* **12**, 634 (2013).
- [17] C.-L. Song, H.-M. Zhang, Y. Zhong, X.-P. Hu, S.-H. Ji, L. Wang, K. He, X.-C. Ma, and Q.-K. Xue, ArXiv e-prints (2015), [arXiv:1511.02007 \[cond-mat.supr-con\]](#).
- [18] Z. R. Ye, C. F. Zhang, H. L. Ning, W. Li, L. Chen, T. Jia, M. Hashimoto, D. H. Lu, Z.-X. Shen, and Y. Zhang, ArXiv e-prints (2015), [arXiv:1512.02526 \[cond-mat.supr-con\]](#).
- [19] Y.-Y. Xiang, F. Wang, D. Wang, Q.-H. Wang, and D.-H. Lee, *Phys. Rev. B* **86**, 134508 (2012).
- [20] S.-H. Baek, D. V. Efremov, J. M. Ok, J. S. Kim, J. van den Brink, and B. Büchner, *Nat Mater* **14**, 210 (2015).
- [21] S.-H. Baek, D. V. Efremov, J. M. Ok, J. S. Kim, J. van den Brink, and B. Büchner, ArXiv e-prints (2015), [arXiv:1510.07533 \[cond-mat.supr-con\]](#).
- [22] M. A. Metlitski, D. F. Mross, S. Sachdev, and T. Senthil, *Phys. Rev. B* **91**, 115111 (2015).
- [23] T. A. Maier and D. J. Scalapino, ArXiv e-prints (2014), [arXiv:1405.5238 \[cond-mat.supr-con\]](#).
- [24] S. Lederer, Y. Schattner, E. Berg, and S. A. Kivelson, *Phys. Rev. Lett.* **114**, 097001 (2015).
- [25] S. Graser, T. A. Maier, P. J. Hirschfeld, and D. J. Scalapino, *New Journal of Physics* **11**, 025016 (2009).
- [26] H. Yamase and R. Zeyher, *Phys. Rev. B* **88**, 180502 (2013).
- [27] K. Jiang, J. Hu, H. Ding, and Z. Wang, ArXiv e-prints (2015), [arXiv:1508.00588 \[cond-mat.supr-con\]](#).
- [28] E. Berg, M. A. Metlitski, and S. Sachdev, *Science* **338**, 1606 (2012).
- [29] Y. Schattner, S. Lederer, S. A. Kivelson, and E. Berg, ArXiv e-prints (2015), [arXiv:1511.03282 \[cond-mat.supr-con\]](#).
- [30] S. Raghu, X.-L. Qi, C.-X. Liu, D. J. Scalapino, and S.-C. Zhang, *Phys. Rev. B* **77**, 220503 (2008).
- [31] K. Binder and D. P. Landau, *Phys. Rev. B* **21**, 1941 (1980); J. Yin and D. P. Landau, *Phys. Rev. E* **80**, 051117 (2009).
- [32] J. E. Hirsch, *Phys. Rev. B* **31**, 4403 (1985).
- [33] R. Blankenbecler, D. J. Scalapino, and R. L. Sugar, *Phys. Rev. D* **24**, 2278 (1981).
- [34] S. R. White, D. J. Scalapino, R. L. Sugar, E. Y. Loh, J. E. Gubernatis, and R. T. Scalettar, *Phys. Rev. B* **40**, 506 (1989).
- [35] F. Assaad and H. Evertz, in *Computational Many-Particle Physics*, Lecture Notes in Physics, Vol. 739, edited by H. Fehske, R. Schneider, and A. Weiße (Springer Berlin Heidelberg, 2008) pp. 277–356.
- [36] W. H. Press, S. A. Teukolsky, W. Vetterling, and B. Flannery, *Numerical recipes, 3rd edn. The art of scientific computing* (Cambridge University Press, Cambridge, 2007).
- [37] Z. Bai, C. Lee, R.-C. Li, and S. Xu, *Linear Algebra and its Applications* **435**, 659 (2011).
- [38] E. Y. J. Loh, J. E. Gubernatis, D. J. Scalapino, R. L. Sugar, S. R. White, and R. T. Scalettar, *Stable simulations of many fermion systems*, Tech. Rep. (United States, 1989).
- [39] H. G. Katzgraber, S. Trebst, D. A. Huse, and M. Troyer, *Journal of Statistical Mechanics: Theory and Experiment* **2006**, P03018 (2006).
- [40] Details of the numerical implementation and benchmarks will be given elsewhere.
- [41] K. Binder, *Zeitschrift für Physik B Condensed Matter* **43**, 119 (1981).
- [42] H. Kontani and S. Onari, *Phys. Rev. Lett.* **104**, 157001 (2010).
- [43] Z.-X. Li, F. Wang, H. Yao, and D.-H. Lee, ArXiv e-prints (2015), [arXiv:1512.06179 \[cond-mat.supr-con\]](#).
- [44] Z.-X. Li, F. Wang, H. Yao, and D.-H. Lee, ArXiv e-prints (2015), [arXiv:1512.04541 \[cond-mat.supr-con\]](#).
- [45] Y. Schattner, M. H. Gerlach, S. Trebst, and E. Berg, ArXiv e-prints (2015), [arXiv:1512.07257 \[cond-mat.supr-con\]](#).